Enhanced Far-Field Thermal Radiation through a Polaritonic Waveguide

Saeko Tachikawa,[1,2,*] Jose Ordonez-Miranda,[1,3,*] Laurent Jalabert,[1,3] Yunhui Wu,[1] Roman Anufriev,[1,4] Yangyu Guo,[1] Byunggi Kim,[1] Hiroyuki Fujita,[1,3] Sebastian Volz,[1,3] and Masahiro Nomura[1,2,3,†]

[1]*Institute of Industrial Science, The University of Tokyo, Tokyo 153-8505, Japan*

[2]*Research Center for Advanced Science and Technology, The University of Tokyo, Tokyo 153-8505, Japan*

[3]*LIMMS, CNRS-IIS IRL 2820, The University of Tokyo, Tokyo 153-8505, Japan*

[4]*Univ. Lyon, INSA Lyon, CNRS, CETHIL, UMR5008, 69621 Villeurbanne, France*

(Received 18 November 2023; revised 3 February 2024; accepted 13 March 2024; published 3 May 2024)

We experimentally demonstrate the enhancement of the far-field thermal radiation between two nonabsorbent Si microplates coated with energy-absorbent silicon dioxide (SiO_2) nanolayers supporting the propagation of surface phonon polaritons. By measuring the radiative thermal conductance between two coated Si plates, we find that its values are twice those obtained without the SiO_2 coating. This twofold increase results from the hybridization of polaritons with guided modes inside Si and is well predicted by fluctuational electrodynamics and an analytical model based on a two-dimensional density of polariton states. These findings could be applied to thermal management in microelectronics, silicon photonics, energy conversion, atmospheric sciences, and astrophysics.

DOI: 10.1103/PhysRevLett.132.186904

Radiative heat transfer between two bodies is an essential phenomenon in our daily lives and in technology. While sunlight powers life on Earth, thermal radiation also plays a key role in thermophotovoltaic energy conversion [1–3], radiative cooling [4–9], and other applications [10–12]. The classical radiative heat transfer is described by Planck's theory [13], which establishes an upper limit for the radiative heat flux between two macroscopic bodies separated by a distance much longer than the dominant radiation wavelength λ_{th} (far-field regime). This Planck's limit can, however, be exceeded under two conditions. First, when the distance between two bodies is smaller than λ_{th} ($\approx$10 μm at room temperature) [14–21]. This near-field radiation thus typically involves radiating surfaces separated by nanogaps and is dominated by the transmission of evanescent electromagnetic waves able to enhance the radiative heat flux by orders of magnitude over Planck's limit [22–28]. The second condition states that this limit can also be overcome with the far-field radiation between two bodies whose dimensions are smaller than λ_{th}. This phenomenon was predicted theoretically [29,30] and experimentally demonstrated for suspended silicon nitrate (SiN) nanofilms with a subwavelength thickness [31,32]. This far-field enhancement can exceed Planck's limit by more than 2 orders of magnitude and is explained by the utilization of energy absorbent nanomaterials supporting the in-plane propagation of electromagnetic waves called surface phonon polaritons (SPhPs) generated by the hybridization of photons and optical phonons [33–36].

In suspended nanofilms, SPhPs can propagate typical distances of a few millimeters, making them powerful energy carriers capable of conducting even more heat than phonons [33–35]. Experiments with suspended silicon dioxide (SiO_2) [37] and SiN [38] nanofilms showed that the SPhP contribution to the heat conduction can double their in-plane thermal conductivity for sufficiently thin or hot nanofilms. Therefore, the emission of this SPhP thermal energy at the edge of a nanofilm and its absorption by another one is expected to significantly enhance the radiative heat transfer, even in the far-field regime, as was experimentally demonstrated for suspended SiN nanofilms [31,32]. However, the role of supported polar nanofilms in the enhancement of far-field radiation remains unknown, as it has never been tackled either experimentally or theoretically, despite their interest in practical applications.

In this Letter, we experimentally demonstrate the enhancement of the far-field radiation between two silicon (Si) microplates coated with SiO_2 nanofilms supporting the propagation of SPhPs. This SPhP-based increase is revealed by the measurement of the radiative thermal conductance between two coated Si plates and the comparison of its values with those obtained in the absence of the SiO_2 nanolayers. In contrast with previous works dealing with absorbent nanofilms [31,32], we thus show that SPhPs can enhance the far-field radiation between nonabsorbent microbodies.

We fabricated three samples to experimentally quantify the radiative heat transfer between two bodies. Each sample consists of two suspended 10-μm-thick intrinsic Si plates separated by a gap, as shown in Fig. 1. The relative permittivity of these nonabsorbing Si microplates is around 11.7, within a broad range of relevant frequencies [39]. To experimentally probe the impact of an oxide coating on radiative heat transfer, the top and bottom surfaces of two Si

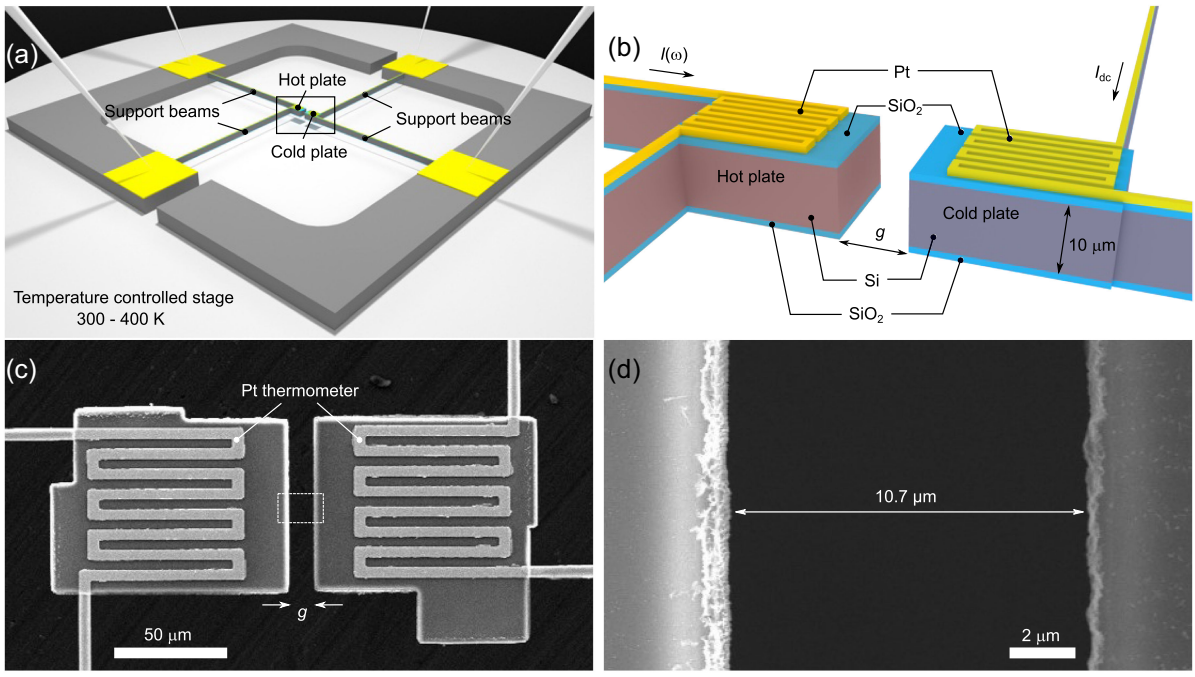

FIG. 1. Experimental platform used to probe the radiative heat transfer. (a) Scheme of two Si microplates suspended by 706-μm-long beams and mounted on a heating stage controlling their temperature. (b) Diagram of the hot and cold plates coated with SiO_2 nanolayers and separated by a vacuum gap $g = 10.7$ μm. Scanning electron microscope image of the (c) device and (d) its close-up on the rectangular box in (c).

plates were coated with SiO_2 nanolayers of 30 and 70 nm in thickness, while the third was kept uncoated to be used as reference [Fig. 1(b)]. Since SiO_2 is a polar material that absorbs energy [Im(permittivity) > 0, Fig. S5(b) of Supplemental Material (SM) [40]], these SiO_2 nanolayers support the thermal excitation of SPhPs and therefore they are expected to convert the coated Si plates into guides of electromagnetic modes able to enhance the thermal radiation, as shown below. One of the plates (hot plate) was heated up, and the other (cold plate) experienced a temperature increase caused by absorbing the thermal radiation emitted from the hot plate. The temperature of both plates was measured via platinum (Pt) serpentine resistors integrated on top of both plates [Fig. 1(c)]. A separation gap of $g = 10.7$ μm [Fig. 1(d)] was set to ensure far-field radiation and neglect near-field effects, as detailed in Sec. 1 of SM [40]. All samples were placed in a vacuum chamber with a pressure of less than 10^{-3} Pa to suppress heat conduction and convection between plates by means of residual air molecules at negligible levels [41].

The samples were fabricated from a silicon-on-insulator wafer, having a top layer of 10 μm in thickness, a buried SiO_2 layer of 2 μm, and a handle layer of 300 μm. First, a backside etching was performed by deep reactive ion etching using an aluminum mask patterned on the backside by photolithography. The buried SiO_2 layer worked as an etch stop. The wafer was cleaned and the buried SiO_2 layer was removed in a buffered hydrofluoric acid. Except for the reference sample, the coating SiO_2 nanolayers with thicknesses of 30 and 70 nm were grown on both sides of each Si plate by dry thermal oxidation at 850 °C (for 90 min) and 1000 °C (for 90 min), respectively. The chromium-platinum (10 nm/100 nm) microresistances were patterned by using sputtering deposition and lift-off. The top Si structures (beams and microresistance platforms) were defined by front-side plasma etching to remove the top SiO_2 nanolayer, the 10-μm-Si layer, and the bottom SiO_2 nanolayer. The remaining photoresist mask was successively removed by oxygen plasma etching as a final step.

We measured the temperatures of the plates by using the 3ω method [25,31,36,42], detailed in Sec. 2 of SM [40]. The hot plate was heated by a sinusoidal electrical current $I(\omega)$, oscillating with an angular frequency ω and circulating along its serpentine Pt wire. The resulting Joule heating then generates a temperature rise $\Delta T_h(2\omega)$ that oscillates with frequency 2ω. The thermal radiation from the hot plate heated up the cold one, whose temperature rise, $\Delta T_c(2\omega)$, was measured by flowing a dc electrical current along its Pt wire and recording the voltage fluctuations at 2ω. The effective thermal conductance G_g of the gap between the hot and cold plates was then determined by applying the principle of energy conservation, which establishes that (Sec. 3 of SM [40])

$$G_g = P_{dc} \frac{\Delta T_c}{(\Delta T_h^2 - \Delta T_c^2)}, \quad (1)$$

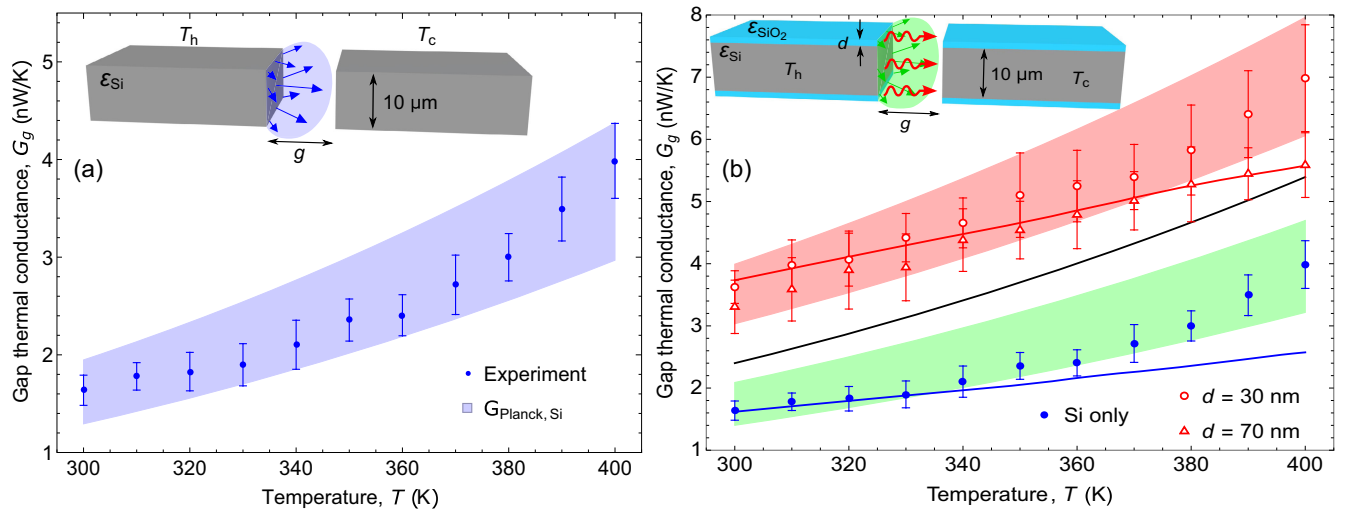

FIG. 2. Experimental and theoretical values of the radiative thermal conductance through the gap between two (a) uncoated and (b) coated Si microplates. The blue zone in (a) represents the prediction of Planck's theory for the far-field thermal conductance $G_{\text{Planck,Si}}$ determined with a Si emissivity $\epsilon_{\text{Si}} = 0.7$ to 0.9. The green and red zones in (b) show the respective predictions of Planck's theory ($G_{\text{Planck,coated Si}}$) and Eq. (2) for the coated Si plate, while the corresponding blue and red lines are computed with fluctuational electrodynamics. The blackbody limit ($\epsilon_{\text{Si}} = \epsilon_{\text{SiO}_2} = 1$) is also shown via the black line. The error bars represent the standard deviations of multiple measurements with different input currents and modulation frequencies.

where P_{dc} is the dc component of the total power generated by the Pt resistor of the hot plate. In deriving Eq. (1), we have taken into account the losses caused by thermal radiation and heat conduction through the support beams. As SiO_2 is a polar material that supports the propagation of SPhPs, while Si does not, we determined the SPhP contribution to the radiative heat transfer by comparing the values of G_g for samples with and without the SiO_2 nanolayers.

To benchmark our measurements against Planck's theory, we first measured the thermal conductance G_g between two uncoated Si plates (Si-only system), as shown in Fig. 2(a). Note that the increase of G_g with the stage temperature T is in good agreement with the predictions of Planck's theory, for the whole range of considered temperatures from 300 to 400 K. This agreement validates our measurements and indicates that the thermal radiation between the uncoated Si plates separated by a 10.7-μm gap is dominated by far-field effects. On the other hand, Fig. 2(b) shows the measured thermal conductance between two Si plates coated with SiO_2 nanolayers. The measured G_g exhibits an increase with temperature similar to that observed for the Si-only system, however, its values (red open points) are nearly twice those obtained for the Si-only system (blue circles). This twofold enhancement is pretty much independent of the thickness (30 and 70 nm) of the SiO_2 nanolayers that support the excitation of SPhPs. This thickness independence is related to the relatively long propagation length of SPhPs that allows them to propagate equally well along the whole surfaces for both coating thicknesses, as shown in Sec. 6 of SM [40].

To explore if the observed far-field radiation is predicted by Planck's theory, we used this theory to calculate the thermal conductance $G_{\text{Planck,coated Si}}$ between two coated Si plates (Sec. 5 of SM [40]) and plotted the obtained results in Fig. 2(b) (green zone). Calculations were done with a SiO_2 emissivity equal to unity to estimate the maximum possible heat exchange between the coated Si plates. For a given temperature, the calculated value of $G_{\text{Planck,coated Si}}$ is only slightly higher than that of $G_{\text{Planck,Si}}$ obtained for the Si-only system [blue zone in Fig. 2(a)]. The negligible difference $G_{\text{Planck,coated Si}} - G_{\text{Planck,Si}}$ is due to the relatively small radiating areas of the SiO_2 nanolayers, which are 140 and 330 times thinner than the Si layer. For comparison and following previous works [30,31], we also calculated the blackbody limit ($\epsilon_{\text{Si}} = \epsilon_{\text{SiO}_2} = 1$) shown by the black line in Fig. 2(b). Note that the measured conductance G_g between the coated Si plates is significantly higher than both the blackbody limit and $G_{\text{Planck,coated Si}}$, which suggests that our experimental far-field observations cannot be explained by the classical Planck's theory based on a geometrical cross section.

To quantitatively compare our experimental data with the predictions of well-established fluctuational electrodynamics, we used the Scuff-EM solver [43] to compute G_g. This electromagnetic solver determines the spectral spatially integrated flux $\Phi(\omega)$ driving the transmission of thermal radiation between the Si plates and therefore the values of G_g, as detailed in section 14 of SM [40]. Figure 3(a) shows the spectra of $\Phi(\omega)$ obtained for the Si plates with and without the SiO_2 coating. One can see that the presence of this coating results in a sharp transmission peak at about

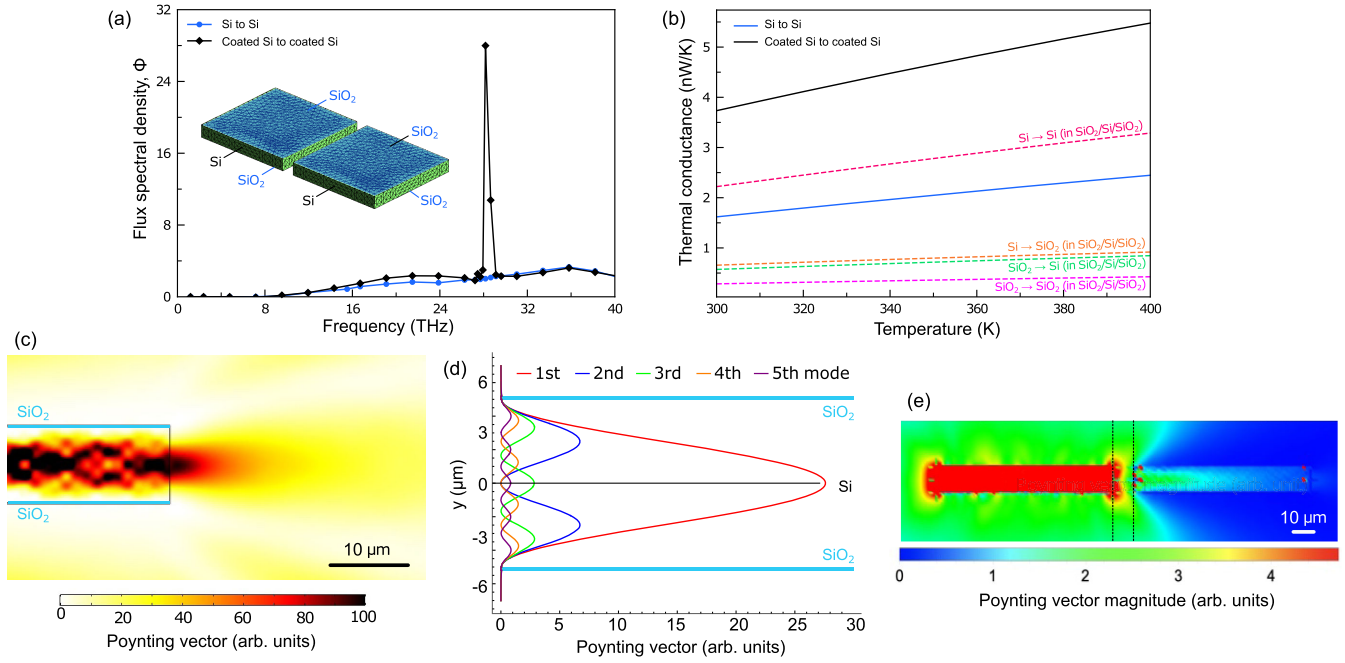

FIG. 3. (a) Generalized flux spectrum for two coated and uncoated Si plates and (b) their corresponding thermal conductance calculated via Scuff-EM. (c) Density map of the in-plane Poynting vector for a coated Si plate showing the dominant in-plane emission of the electromagnetic flux. (d) Poynting vector components arising from the propagation of multiple guided modes inside the Si layer mainly. (e) Density map of the Poynting vector magnitude obtained for two facing coated Si plates. Calculations were done for $\omega/2\pi = 28$ THz, for which SPhPs exhibit the resonant transmission shown in (a).

28 THz (176 Trad/s), which maximizes the SPhP propagation distance [Supplemental Material, Fig. S7(b) [40]] due to the minimum energy absorption of SiO_2, as set by the imaginary part of its permittivity shown in Fig. S5(b) of SM [40]. The longest SPhP propagation length along the coated Si plate thus enhances its heat transfer through the gap. The resonant transmission between the Si plates hence arises from their SiO_2 coating, as bare Si does not support the propagation of SPhPs. The integration of $\Phi(\omega)$ weighted by the Bose-Einstein distribution over all frequencies indicates that the $\Phi(\omega)$ peak nearly doubles the total thermal conductance between the Si plates, as shown in Fig. 3(b). The thermal conductance between the coated Si plates was calculated by summing its components for the radiation exchanged between different layers at the hot and cold sides ($Si \rightarrow Si + Si \rightarrow SiO_2 + SiO_2 \rightarrow Si + SiO_2 \rightarrow SiO_2$). Note that the major contribution to the thermal radiation between the coated Si plates arises from that of the core Si plates, which in the presence of coating, exchange more thermal energy than two uncoated Si plates. The SiO_2 nanocoating therefore enhances the thermal radiation between the Si microplates, without modifying their inner structure. More importantly, the calculated total thermal conductance between two coated Si plates is in good agreement with our experimental data, as shown in Fig. 2(b). The observed deviations between theory and experiments for temperatures close to 400 K mainly arise from the high-frequency convergence issues we found during the Scuff-EM simulations, as they are present for both the coated and uncoated Si plates.

To correlate the improvement in gap thermal conductance with the excitation of SPhPs along a coated Si plate, we analyzed the spatial distribution of their energy density. By solving the Maxwell equations for the transverse magnetic polarization allowing the predominant propagation of SPhPs, we obtained the in-plane component of the Poynting vector inside and outside the coated Si plate, as shown in Fig. 3(c). Note that the electromagnetic flux is mainly propagating inside the nonabsorbent Si layer via guided modes [Fig. 3(d)] hybridized with SPhPs excited in the SiO_2 nanolayers. The first mode exhibits the highest amplitude, which decreases as the mode order increases. The electromagnetic flux of the modes inside the hot system is guided along the in-plane direction and is mainly emitted into the vacuum that separates it from the cold system. This fact is further confirmed by the spatial distribution of the Poynting vector magnitude (including in-plane and cross-plane components) shown in Fig. 3(e) for two facing coated Si plates. Even though most of the energy is concentrated inside the hot Si layer, there is some energy outside of it and therefore the effective cross section of the heater may be greater than its geometrical one. However, the energy guided by this hot layer is emitted to and absorbed by the cold Si layer via its geometrical cross section predominantly. This limited absorption cross section of the sensor recording our measurements thus

suggests that our results cannot be explained by an extended cross section. Further, the influence of Pt thermometers on the in-plane emission is negligible (Sec. 8 of SM [40]), which indicates that hybridized guided modes are expected to explain the enhanced thermal radiation shown in Fig. 2(b).

Considering that the heat transfer through the gap between two coated Si plates consists not only of the classical far-field radiation between the facing surfaces but also of the in-plane emission of the guided modes hybridized with SPhPs, the total thermal conductance through the gap can be modeled as follows:

$$G = G_{\text{Planck,coated Si}} + G_{\text{SPhPs}}, \tag{2}$$

where G_{SPhPs} is the thermal conductance due to the emission of the SPhP energy. Taking into account the dominant in-plane propagation of SPhPs [Fig. 3(d)], their description in terms of a two-dimensional (2D) density of states yields (Sec. 9 of SM [40])

$$G_{\text{SPhPs}} = \frac{\epsilon\sigma_{2\text{D}} a (T_{\text{h}}^3 - T_{\text{c}}^3)}{T_{\text{h}} - T_{\text{c}}}, \tag{3}$$

where $\epsilon = \epsilon_{\text{coated Si}}/(F^{-1} + 1 - \epsilon_{\text{coated Si}})$, $\sigma_{2\text{D}} = 4z(3)k_B^3/ch^2 \approx 9.6 \times 10^{-11}$ W m^{-1} K^{-3}, $a = 78$ μm is the width of the plate, $\epsilon_{\text{coated Si}}$ is the effective emissivity of the coated Si plate, F is its corresponding view factor, $z(3)$ is the zeta function, and k_B and h are the Boltzmann and Planck constants, respectively. As the radiation area of the Si microplates is more than 100 times larger than that of the SiO_2 nanolayers, we estimate the values of G_{SPhPs} using the approximations $\epsilon_{\text{coated Si}} \approx \epsilon_{\text{Si}} = 0.7$–$0.9$ and $F \approx 0.9$–1.0, appropriate for the 2D SPhP propagation (Secs. 9 and 10 of SM [40]). The total thermal conductance G thus predicted by Eq. (2) embraces well its corresponding experimental values, as shown by the red zone in Fig. 2(b). This agreement points out that the proposed model for the superposition of the 3D + 2D radiation can describe the emission of the SPhP modes guided along the coated Si plate. This is further confirmed by the fact that Eqs. (2) and (3) also predict well the measured thermal conductance for the far-field radiation between two SiN nanofilms reported in the literature [31] (Sec. 11 of SM [40]). The consistency of our experimental and theoretical results thus indicates that the coated Si microplates are efficient waveguides to transfer thermal energy and enhance their far-field radiation along the in-plane direction.

In summary, we have experimentally demonstrated that the polariton guided modes double the far-field thermal radiation between two microplates of Si coated with SiO_2 nanolayers. This enhancement is explained by the excitation of SPhP modes inside the energy-absorbent SiO_2 nanolayers and their hybridization with guided resonant modes propagating mainly within the nonabsorbent Si plates. Our experimental results align closely with both the numerical predictions of fluctuational electrodynamics and an analytical model based on a two-dimensional density of polariton states. In contrast to the previous studies working with subwavelength absorbent structures [25,31,32], our finding uncovers the potential of SPhPs to enhance far-field radiation between nonabsorbent coated bodies, even when their dimensions are comparable to or greater than the dominant radiation wavelength. This thermal radiation enhancement obtained with Si-based micromaterials of a simple geometry could thus have broad applications in microelectronics and semiconductor fields.

The authors thank Professor Hiroshi Toshiyoshi for allowing us the access to his clean room facilities. This work was supported by the CREST JST (Grants No. JPMJCR19Q3 and No. JPMJCR19I1) and KAKENHI JSPS (Grants No. 21H04635 and No. JP20J13729) projects, as well as by the JSPS Core-to-Core Program (Grant No. JPJSCCA20190006). We also thank Olivier Merchiers for his advice on Scuff-EM simulations.

*These authors contributed equally to this work.
†nomura@iis.u-tokyo.ac.jp

[1] S. Fan, An alternative "sun" for solar cells, Nat. Nanotechnol. **9**, 92 (2014).
[2] D. Fan, T. Burger, S. McSherry, B. Lee, A. Lenert, and S. R. Forrest, Near-perfect photon utilization in an air-bridge thermophotovoltaic cell, Nature (London) **586**, 237 (2020).
[3] R. Mittapally, B. Lee, L. Zhu, A. Reihani, J. W. Lim, D. Fan, S. R. Forrest, P. Reddy, and E. Meyhofer, Near-field thermophotovoltaics for efficient heat to electricity conversion at high power density, Nat. Commun. **12**, 4364 (2021).
[4] Y. De Wilde and R. Haidar, Optical cooling achieved by tuning thermal radiation, Nature (London) **566**, 186 (2019).
[5] T. Li, Y. Zhai, S. He, W. Gan, Z. Wei, M. Heidarinejad, D. Dalgo, R. Mi, X. Zhao, J. Song *et al.*, A radiative cooling structural material, Science **364**, 760 (2019).
[6] L. Zhu, A. Fiorino, D. Thompson, R. Mittapally, E. Meyhofer, and P. Reddy, Near-field photonic cooling through control of the chemical potential of photons, Nature (London) **566**, 239 (2019).
[7] J. Song, J. Seo, J. Han, J. Lee, and B. J. Lee, Ultrahigh emissivity of grating-patterned PDMS film from 8 to 13 μm wavelength regime, Appl. Phys. Lett. **117**, 094101 (2020).
[8] T. Sadi, I. Radevici, and J. Oksanen, Thermophotonic cooling with light-emitting diodes, Nat. Photonics **14**, 205 (2020).
[9] J. Li, Y. Liang, W. Li, N. Xu, B. Zhu, Z. Wu, X. Wang, S. Fan, M. Wang, and J. Zhu, Protecting ice from melting under sunlight via radiative cooling, Sci. Adv. **8**, eabj9756 (2022).
[10] S. H. Yun and S. J. Kwok, Light in diagnosis, therapy and surgery, Nat. Biomed. Eng. **1**, 0008 (2017).
[11] M. Bocková, J. Slabý, T. Špringer, and J. Homola, Advances in surface plasmon resonance imaging and microscopy and

their biological applications, Annu. Rev. Analy. Chem. **12**, 151 (2019).
[12] R. Pacelli, M. Caroprese, G. Palma, C. Oliviero, S. Clemente, L. Cella, and M. Conson, Technological evolution of radiation treatment: Implications for clinical applications, in *Seminars in Oncology* (2019), Vol. 46, pp. 193–201.
[13] M. Planck, The theory of heat radiation, Entropie **144**, 164 (1900).
[14] D. Polder and M. Van Hove, Theory of radiative heat transfer between closely spaced bodies, Phys. Rev. B **4**, 3303 (1971).
[15] K. Joulain, J.-P. Mulet, F. Marquier, R. Carminati, and J.-J. Greffet, Surface electromagnetic waves thermally excited: Radiative heat transfer, coherence properties and Casimir forces revisited in the near field, Surf. Sci. Rep. **57**, 59 (2005).
[16] J.-P. Mulet, K. Joulain, R. Carminati, and J.-J. Greffet, Enhanced radiative heat transfer at nanometric distances, Microscale Thermophys. Eng. **6**, 209 (2002).
[17] A. Kittel, Probing near-field thermal radiation, Nat. Photonics **3**, 492 (2009).
[18] S. Basu, B. J. Lee, and Z. M. Zhang, Near-field radiation calculated with an improved dielectric function model for doped silicon, J. Heat Transfer **132**, 023302 (2010).
[19] M. Nomura, The heat through the gap, Nat. Nanotechnol. **11**, 496 (2016).
[20] K. Isobe, D. Hirashima, and K. Hanamura, Spectrally enhanced near-field radiation transfer using nanometer-sized pillar array structured surfaces, Int. J. Heat Mass Transfer **115**, 467 (2017).
[21] K. Ito, K. Nishikawa, A. Miura, H. Toshiyoshi, and H. Iizuka, Dynamic modulation of radiative heat transfer beyond the blackbody limit, Nano Lett. **17**, 4347 (2017).
[22] E. Rousseau, A. Siria, G. Jourdan, S. Volz, F. Comin, J. Chevrier, and J.-J. Greffet, Radiative heat transfer at the nanoscale, Nat. Photonics **3**, 514 (2009).
[23] R. S. Ottens, V. Quetschke, S. Wise, A. A. Alemi, R. Lundock, G. Mueller, D. H. Reitze, D. B. Tanner, and B. F. Whiting, Near-field radiative heat transfer between macroscopic planar surfaces, Phys. Rev. Lett. **107**, 014301 (2011).
[24] K. Kim, B. Song, V. Fernández-Hurtado, W. Lee, W. Jeong, L. Cui, D. Thompson, J. Feist, M. H. Reid, F. J. García-Vidal *et al.*, Radiative heat transfer in the extreme near field, Nature (London) **528**, 387 (2015).
[25] B. Song, D. Thompson, A. Fiorino, Y. Ganjeh, P. Reddy, and E. Meyhofer, Radiative heat conductances between dielectric and metallic parallel plates with nanoscale gaps, Nat. Nanotechnol. **11**, 509 (2016).
[26] M. Lim, J. Song, S. S. Lee, and B. J. Lee, Tailoring near-field thermal radiation between metallo-dielectric multilayers using coupled surface plasmon polaritons, Nat. Commun. **9**, 4302 (2018).
[27] J. DeSutter, L. Tang, and M. Francoeur, A near-field radiative heat transfer device, Nat. Nanotechnol. **14**, 751 (2019).
[28] A. Fiorino, D. Thompson, L. Zhu, R. Mittapally, S.-A. Biehs, O. Bezencenet, N. El-Bondry, S. Bansropun, P. Ben-Abdallah, E. Meyhofer *et al.*, A thermal diode based on nanoscale thermal radiation, ACS Nano **12**, 5774 (2018).
[29] S.-A. Biehs and P. Ben-Abdallah, Revisiting super-Planckian thermal emission in the far-field regime, Phys. Rev. B **93**, 165405 (2016).
[30] V. Fernández-Hurtado, A. I. Fernández-Domínguez, J. Feist, F. J. García-Vidal, and J. C. Cuevas, Super-Planckian far-field radiative heat transfer, Phys. Rev. B **97**, 045408 (2018).
[31] D. Thompson, L. Zhu, R. Mittapally, S. Sadat, Z. Xing, P. McArdle, M. M. Qazilbash, P. Reddy, and E. Meyhofer, Hundred-fold enhancement in far-field radiative heat transfer over the blackbody limit, Nature (London) **561**, 216 (2018).
[32] D. Thompson, L. Zhu, E. Meyhofer, and P. Reddy, Nanoscale radiative thermal switching via multi-body effects, Nat. Nanotechnol. **15**, 99 (2020).
[33] D.-Z. A. Chen, A. Narayanaswamy, and G. Chen, Surface phonon-polariton mediated thermal conductivity enhancement of amorphous thin films, Phys. Rev. B **72**, 155435 (2005).
[34] J. Ordonez-Miranda, L. Tranchant, T. Tokunaga, B. Kim, B. Palpant, Y. Chalopin, T. Antoni, and S. Volz, Anomalous thermal conductivity by surface phonon-polaritons of polar nano thin films due to their asymmetric surrounding media, J. Appl. Phys. **113**, 084311 (2013).
[35] M. Lim, J. Ordonez-Miranda, S. S. Lee, B. J. Lee, and S. Volz, Thermal-conductivity enhancement by surface electromagnetic waves propagating along multilayered structures with asymmetric surrounding media, Phys. Rev. Appl. **12**, 034044 (2019).
[36] S. Shin, M. Elzouka, R. Prasher, and R. Chen, Far-field coherent thermal emission from polaritonic resonance in individual anisotropic nanoribbons, Nat. Commun. **10**, 1377 (2019).
[37] L. Tranchant, S. Hamamura, J. Ordonez-Miranda, T. Yabuki, A. Vega-Flick, F. Cervantes-Alvarez, J. J. Alvarado-Gil, S. Volz, and K. Miyazaki, Two-dimensional phonon polariton heat transport, Nano Lett. **19**, 6924 (2019).
[38] Y. Wu, J. Ordonez-Miranda, S. Gluchko, R. Anufriev, D. D. S. Meneses, L. Del Campo, S. Volz, and M. Nomura, Enhanced thermal conduction by surface phonon-polaritons, Sci. Adv. **6**, eabb4461 (2020).
[39] E. D. Palik, *Handbook of Optical Constants of Solids* (Academic Press, New York, 1998), Vol. 3.
[40] See Supplemental Material at http://link.aps.org/supplemental/10.1103/PhysRevLett.132.186904 for the detailed description of the theoretical background and the analysis of our experimental results.
[41] K. Ito, K. Nishikawa, H. Iizuka, and H. Toshiyoshi, Experimental investigation of radiative thermal rectifier using vanadium dioxide, Appl. Phys. Lett. **105**, 253503 (2014).
[42] B. Song, Y. Ganjeh, S. Sadat, D. Thompson, A. Fiorino, V. Fernández-Hurtado, J. Feist, F. J. Garcia-Vidal, J. C. Cuevas, P. Reddy *et al.*, Enhancement of near-field radiative heat transfer using polar dielectric thin films, Nat. Nanotechnol. **10**, 253 (2015).
[43] A. W. Rodriguez, M. H. Reid, and S. G. Johnson, Fluctuating-surface-current formulation of radiative heat transfer for arbitrary geometries, Phys. Rev. B **86**, 220302(R) (2012).